Excited state dynamics of protonated dopamine: Hydration and conformation effects

Keisuke Hirata, Ken-Ichi Kasai, Koki Yoshizawa, Gilles Grégoire, Shun-Ichi Ishiuchi, Masaaki Fujii

Excited state dynamics of protonated dopamine: Hydration and conformation effects

Keisuke Hirata,[1, 2, 3] Ken-ichi Kasai,[1, 4] Koki Yoshizawa [1,4] Gilles Grégoire,[3, 5] Shun-ichi Ishiuchi[1, 2, 3]* and Masaaki Fujii[1, 3, 4]**

[1] Laboratory for Chemistry and Life Science, Institute of Innovative Research, Tokyo Institute of Technology, 4259 Nagatsu-ta-cho, Midori-ku, Yokohama, 226-8503, Japan

[2] Department of Chemistry, School of Science, Tokyo Institute of Technology. 2-12-1 4259 Ookayama, Meguro-ku, Tokyo, 152-8550, Japan

[3] Tokyo Tech World Research Hub Initiative (WRHI), Institute of Innovation Research, Tokyo Institute of Technology, 4259, Nagatsuta-cho, Midori-ku, Yokohama, 226-8503, Japan

[4] School of Life Science and Technology, Tokyo Institute of Technology. 4259 Nagatsuta-cho, Midori-ku, Yokohama, Kanagawa, 226-8503, Japan

[5] Université Paris-Saclay, CNRS, Institut des Sciences Moléculaires d'Orsay, F-91405 Orsay, France

E-mail: gilles.gregoire@universite-paris-saclay.fr, ishiuchi.s.aa@m.titech.ac.jp, mfujii@res.titech.ac.jp

ORCID : Keisuke Hirata : 0000-0003-4472-7992, Shun-ichi Ishiuchi : 0000-0002-4079-818X, Gilles Gregoire : 0000-0002-8577-3621, Masaaki Fujii: 0000-0003-4858-4618

KEYWORDS catecholamine, solvation effect, excited state proton transfer, infrared spectroscopy, photodissociation, quantum chemistry calculations

ABSTRACT

Electronic and vibrational spectroscopy in a cryogenic ion trap have been applied to protonated dopamine water clusters and assigned with the help of quantum chemistry calculations performed in the ground and electronic excited states. A dramatic hydration effect is observed when dopamine is solvated by three water molecules. The broad electronic spectra recorded for the bare and small water clusters containing protonated dopamine turn to sharp, well-resolved vibronic transitions in the 1-3 complex. This reflects the change induced by hydration in the photodynamics of protonated dopamine which is initially controlled by an excited state proton transfer (ESPT) reaction from the ammonium group toward the catechol ring. Interestingly, a conformer selectivity is revealed in the 1-3 complex which shows two low lying energy conformers for which the ESPT reaction is prevented or not depending on the H-bond network formed between the dopamine and water molecules.

1 Introduction

Dopamine (DA) is one of catecholamines which has two hydroxyl groups and an amine chain. Biologically, DA as a neurotransmitter plays important roles in homeostasis and addiction, such as motor coordination, memory, reward processes, signal transmission from neurons, relation to Parkinson's disease and so on. DA and related catecholamines show unique photophysical properties originated from multiple photoactive functional groups. The OH groups substituted to phenyl ring provide the hydrogen atom and proton transfers in relation to $\pi\pi^*$ and $\pi\sigma^*$ states.[1-5] An amino group, particularly after protonation also gives proton transfer reaction toward the phenyl ring.[6] When the amine group is not protonated, the nonbonding orbital of the amino group generates a $\pi_{NH2}\pi^*$ state which may induce efficient internal conversion from the photoactive $\pi\pi^*$ state. Competition of these multiple photodynamical processes are characteristic properties of DA and catecholamines and their protonated species. Furthermore, these dynamics are easily affected by conformational variations and solvation because the relative energies of related electronic excited states sensitively varies in H-bonded molecular clusters.[7] The intrinsic conformational varieties of DA, which is strongly related to molecular recognition by DA receptor, has been studied by infrared (IR) spectroscopy in gas phase and theoretical calculations.[8, 9] On the other hand, its photophysical properties have not been understood sufficiently. Under physiological conditions, DA is protonated thus the excited state dynamics of protonated DA (DAH^+) should be studied. In addition, hydration and dehydration effects on its photophysical properties is also important because DAH^+ is hydrated in vivo but have to be dehydrated when it is recognized in the hydrophobic binding pocket of DA receptor.[10] Thus, excited state dynamics of DA, protonated DA and related catecholamines are very good benchmark cases to understand photodynamics in complex molecular systems.

Recently, we have found that the broad UV spectrum of DAH^+ turns to the sharp, well-structured one by hydration of three water molecules.[11] This drastic change of the spectra is rationalized by the excited state proton transfer (ESPT) from the amine group to the catechol ring in bare DAH^+ and its disruption by the insertion of a water molecule between the amine group and the aromatic ring. However, the complete analysis of this unusual dynamical change has not been studied yet. The points that have to be revealed are, the effect of stepwise hydration by a single and two water molecules, sudden opening of the H-loss channel in the triply hydrated DAH^+ and

the role of $\pi_{NH2}\pi^*$ excited state and internal conversion. For this motivation, we have further proceeded to the detailed study on excited state dynamics of hydrated DAH^+ by cryogenic IR and UV ion spectroscopy assigned with the help of theoretical calculations for the ground and excited states, respectively. Relations between the dynamics, structures and electronic states are fully discussed in relation to the stepwise hydration effect.

2 Experimental and Calculation Methods

The experimental setup in Tokyo has already been described in detail.[12] It is based on an electrospray ion source, cold ion trap and time-of-flight mass spectrometer. A methanol solution containing dopamine (Sigma Aldrich, 3.0×10^{-4} M) with 0.5% formic acid is electrosprayed in front of a heated capillary. The ions of interest were transported by a hexapole ion guide and were hydrated in an octupole linear ion trap[13, 14] maintained at 180 K, in which water vapor is introduced by a pulsed valve (Parker Hannifin, General Valve Series 9). The hydrated ions were mass-selected by a quadrupole mass spectrometer (Extrel) and were introduced into a cryogenic quadrupole ion trap (QIT) via a quadrupole ion bender and octupole ion guides. The QIT was kept at 4 K by a closed-cycle two-stage He refrigerator (Sumitomo, RDK-408D2). Helium buffer gas was introduced into the QIT by a pulsed valve (Parker Hannifin, General Valve Series 9) to allow He to collisionally cool the hydrated ions down to ~10 K. The cold ions were irradiated with a tunable dye UV laser (Lumonics) or OPO/OPA IR laser (LaserVision) and the photofragments and parent ions are mass-analyzed in a time-of-flight mass spectrometer. UV/IR photodissociation (UVPD/IRPD) spectra were measured by scanning the yield of the photofragment ions as a function of laser wavenumber. For the hydrates, the moderate binding energies of the water clusters allow recording IRPD spectroscopy by monitoring the water evaporation channel as a function of the IR wavelength. In this latter scheme, the IR spectrum comprises the IR signature of all populated conformers in the cold QIT trap. In order to get a conformer-selected IR spectrum, IR-IR or IR-UV dip spectroscopies should be performed. To measure an IR-UV dip spectrum, a tunable IR laser (LaserVision, OPO/OPA) illuminated the hydrated ions before UV irradiation whose wavenumber was fixed at the band origin of the UVPD spectrum. If the ions are vibrationally excited by the IR laser, the photofragment yield is reduced due to the depopulation of the ground vibrational state. IR-UV dip spectra were thus obtained by monitoring the depletion

of the photofragment signal and gives conformer-selective IR spectra. Similarly, IR-IR dip spectrum is recorded by scanning a first IR laser while the second IR laser is set on a specific transition of the IRPD spectrum. In the latter case, the first IR laser is prone to produce the same photofragment (H_2O loss) as the probe laser, which would preclude to observe the dip in the signal. So the fragment produced by the first IR laser is removed from the QIT by the Tickle method.[15] An auxiliary RF whose frequency is tuned in resonance with the mass of interest (m/z 152 for DAH^+) and sent to the entrance endcap of the QIT during 1 ms to eject the photofragment.

Conformational searches were performed by metadynamics sampling as implemented in the XTB package[16] and using the CREST program.[17] Initial structures were systematically made for each cluster size by adding a water molecule to each conformer of protonated dopamine (G1 and G2 rotamers). Density functional theory calculations were further performed for the structural assignment of the hydrated clusters of protonated dopamine in the electronically ground state (S_0) using TURBOMOLE program package (ver. 7.1).[18] Structural optimization and harmonic frequency calculations were performed at the B3LYP-D3BJ/cc-pVTZ level. The harmonic frequencies were corrected with a scaling factor of 0.956 (for NH and catechol OH stretches), 0.962 (for water OH stretch), and 0.975 (for others).[19, 20] Ab initio CC2 calculations have been performed making use of the resolution-of-the-identity (RI) approximation for the evaluation of the electron-repulsion integrals.[21, 22] The equilibrium geometries of protonated dopamine and its water cluster in the electronic ground (S_0) and first excited (S_1) states have been determined at the spin-component scaled SCS-CC2 level[23] with correlation-consistent polarized valence double-ζ aug-cc-pVDZ basis set augmented with diffuse functions.[24] For the SCS-CC2 calculations, we used the standard scaling factors as implemented in Turbomole (css=1/3, cos=6/5). The vibrational modes of the ground and the first excited states have been calculated at the same level in order to obtain the adiabatic excitation energy corrected for the difference of zero-point energy between the two states. The calculated vibrationally-resolved electronic spectra were obtained with the PGOPHER spectra simulator package[25] using the calculated frequencies of the ground and excited states. For the sake of comparison, the simulation was performed at 0 K and convoluted with a gaussian function of 3 cm^{-1} (full-width at half-maximum FWHM). Finally, the reaction paths connecting the locally excited state with the ESPT structure were predicted at the SCS-CC2 level as implemented in Turbomole using the woelfling program. 10 initial structures were first generated by a Linear Synchronous Transit method and further optimized in order to estimate the

energy of the transition state which defines the height of the ESPT barrier.

3 Results and Discussion

3.1 UV Spectra of DAH^+ and its hydrated clusters

Fig. 1 shows the UV photodissociation spectra of DAH^+ and its hydrated clusters $DAH^+(H_2O)_n$ (n = 0 – 3). All the spectra are obtained by monitoring the intensity of the fragment ion m/z 137, which corresponds to NH_3 + $n$$H_2O$ loss from $DAH^+(H_2O)_n$ (Fig. S1). The UVPD spectrum of DAH^+ (Fig. 1) consists of two sets of broad bands. A low intensity background signal starts below 34 000 cm^{-1} while a more intense transition is centered at 35 000 cm^{-1}. As already reported,[8, 11] two conformers are populated at low temperature, which only differ by the orientation of the alkyl chain above the catechol ring (rotamers G1 and G2). The broadening of the electronic spectrum of DAH^+ has been assigned to a fast relaxation process involving an intramolecular ESPT from the ammonium group towards the catechol ring. Pump-probe photodissociation spectroscopy of DAH^+ points out a very short excited state lifetime, lower the cross correlation of the picosecond lasers.[11]

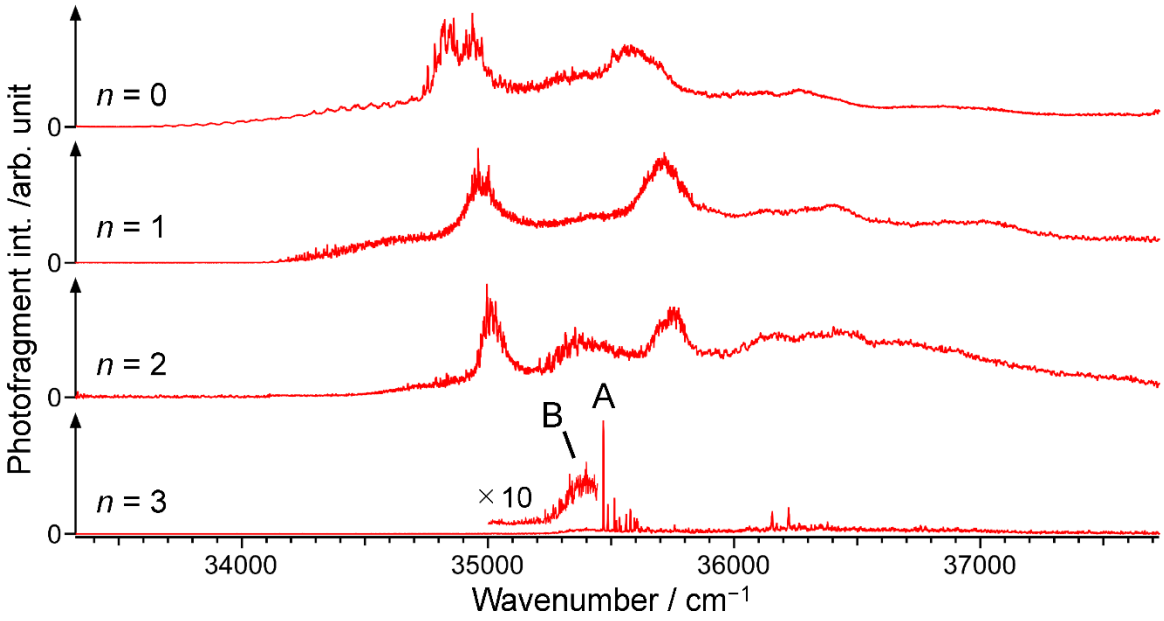

Fig. 1 UVPD spectra of $DAH^+(H_2O)_n$ (n = 0 - 3).

The hydrated clusters $DAH^+(H_2O)_{1,2}$ show similar spectral features, which consist of low intensity

background and intense broadened bands. The spectral feature changes drastically when DAH^+ is hydrated by three water molecules. For this cluster size, vibronic transitions (labelled A in Fig. 1) are now well resolved. Clearly it shows the drastic change of the dynamics in the excited state by addition of the third water molecule. Another important point is the reminiscence of a broad component (labelled B in Fig. 1) from 35 200 cm^{-1} in addition to the sharp bands A in the UVPD spectrum of $DAH^+(H_2O)_3$. This suggests that these two spectral patterns are issued from distinct conformers with different relaxation rates and deactivation processes. We will first analyze the structural differences between A and B conformers of $DAH^+(H_2O)_3$ to understand the significant hydration effect on the relaxation process of DAH^+.

3.2 IR-UV dip spectra of $DAH^+(H_2O)_3$

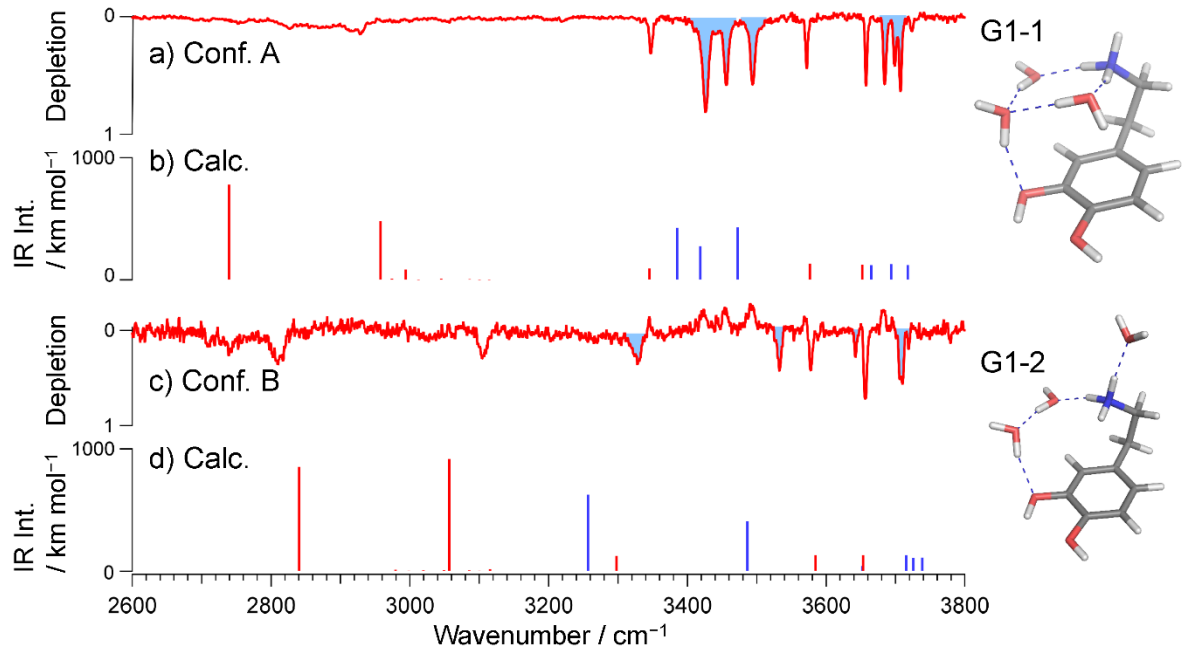

Fig. 2 Observed (a and c) and calculated (b and d) IR dip spectra of $DAH^+(H_2O)_3$. Observed IR spectra (a and c) are obtained by probing the A and B UV transitions in Fig. 1, respectively.

Fig. 2 shows the IR dip spectra of $DAH^+(H_2O)_3$ which are measured by fixing the UV laser to a) the sharp band A at 35 469 cm^{-1} and b) the broad band B at 35 388 cm^{-1}. The IR dip spectroscopy

is a double resonance spectroscopy, which detects the IR transition by depletion of the UVPD signal. The IR spectrum shown in Fig. 2a is measured by setting the UV wavelength on the S_1 origin of conformer A. Blue shaded bands are assigned to OH stretching of water molecules because these bands disappear in the IRPD spectrum of $DAH^+(D_2O)_3$ (Fig. S2). To assign the structure of the cluster, quantum chemical calculations are performed and the 10 lowest energy conformers of $DAH^+(H_2O)_3$ (Table S1) are shown in Fig. S3 along with the theoretical spectra in the 3 μm range in Fig. S4. The structures and theoretical IR spectra of the two most stable conformers G1-1 and G1-2 are shown in Fig. 2b and 2d, respectively. The OH stretching of water molecules in the clusters are shown by blue bars, while other vibrations of DAH^+ are indicated by red bars. As can be seen in Fig. 2b, the theoretical IR spectrum of the most stable conformer G1-1 provides a fair agreement with the observed IR dip spectrum of the conformer A. It should be noted that the set of the three water stretches observed between 3400 and 3500 cm^{-1} is predicted only for the G1-1 conformer, none of the nine other conformers displays such pattern (Fig. S4). The adiabatic excitation energy, corrected by the difference in zero-point-energy between the excited and ground state, is calculated at 34 747 cm^{-1}, only 750 cm^{-1} to the red of the experimental 0_0^0 transition. Besides, the simulated Franck-Condon spectrum of G1-1 also reproduces the main spectral features of the UV spectrum (Fig. 3a). The S_1 origin is the strongest and low frequency bands appear within 400 cm^{-1} from the origin. The active low frequency modes in S_1 are identified as out-of-plane bending of OH catechol and vibrational motions of the hydrated amine chain, as already reported in ref 11. Thus G1-1 can be confidently assigned to the structure of the $DAH^+(H_2O)_3$.

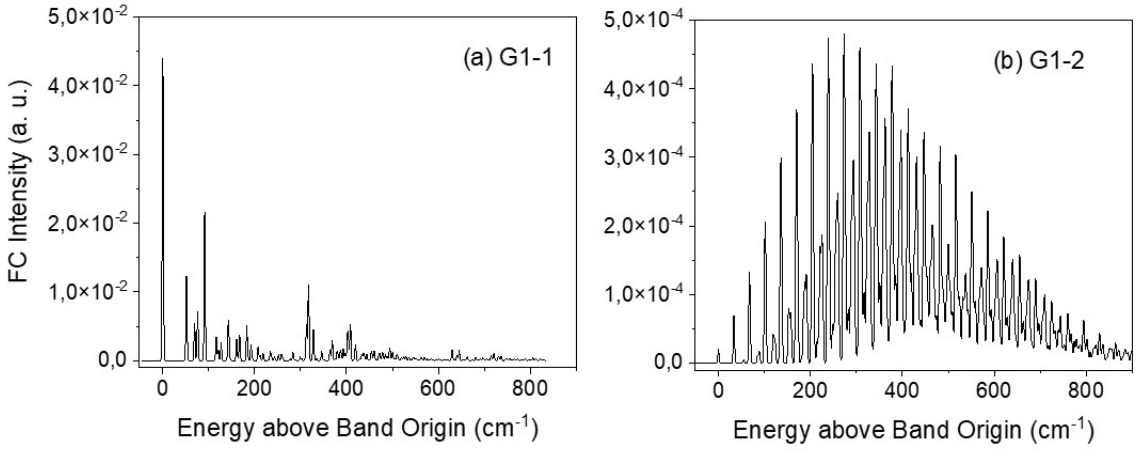

Fig. 3 Calculated Franck-Condon factors of the two conformers (a) G1-1 and (b) G1-2 of DAH^+-$(H_2O)_3$. Note the 100-fold lower intensity for G1-2.

The IR dip spectrum (Fig. 2c) obtained by fixing the UV laser to the broad band B is reasonably reproduced by the second stable conformer G1-2 (Fig. 2d). No other conformers except for G1-4 gives a satisfying theoretical spectrum, in particular to reproduce the set of two NH stretches around 2800 cm^{-1} and 3100 cm^{-1} (Fig. S4). The conformer G1-4 is 8.4 kJ/mol less stable than G1-2 so we tentatively exclude this conformer. The theoretical UV spectrum of G1-2 is shown in Fig. 3b. It shows a long progression of low-frequency vibrations, and the band intensities are spread to a wide frequency range with weak band origin. This is in sharp contrast to the observed and calculated UV spectra of the conformer A but totally consistent with the broad and low intensity absorption band of conformer B. If this conformer has a fast relaxation process, individual transitions will be broadened and the theoretical UV spectrum will be quite similar to the observed broad spectrum.

3.3 IR-IR dip spectra of $DAH^+(H_2O)$

The UV spectrum of $DAH^+(H_2O)$ is unstructured likewise for the monomer and the conformer B of $DAH^+(H_2O)_3$. The IRPD spectrum of $DAH^+(H_2O)$ is reported in Fig. 4a, which displays sharp and well-resolved vibrational transitions. The missing transitions in the IRPD of $DAH^+(D_2O)$ complex (compared to the H_2O complex) reported in Fig. S5 are assigned to the OH stretches of the water molecule. Fig. 4b and 4d show the IR-IR dip spectra obtained by probing b) the band A at 3330 cm^{-1} and c) the band B at 3349 cm^{-1}. These two spectra are different from each other, thus the coexistence of two conformers is established. The six lowest energy conformers of $DAH^+(H_2O)$ are plotted in Fig. S6 along with their Gibbs free energy (180 K) in Table S2 and their predicted IR spectrum in Fig. S7. The most stable (G1-1) and the second most stable (G1-2, ΔG_{180K} = 0.4 kJ/mol) conformations provide fair agreement with the two IR-IR dip spectra in Fig. 4b and 4d, respectively. Besides, their predicted FC spectra (Fig. S8) show long progressions of low frequency modes, consistent with the broad experimental excitation spectrum. From these reasons, we assigned G1-1 and G1-2 conformations for two conformers in $DAH^+(H_2O)$.

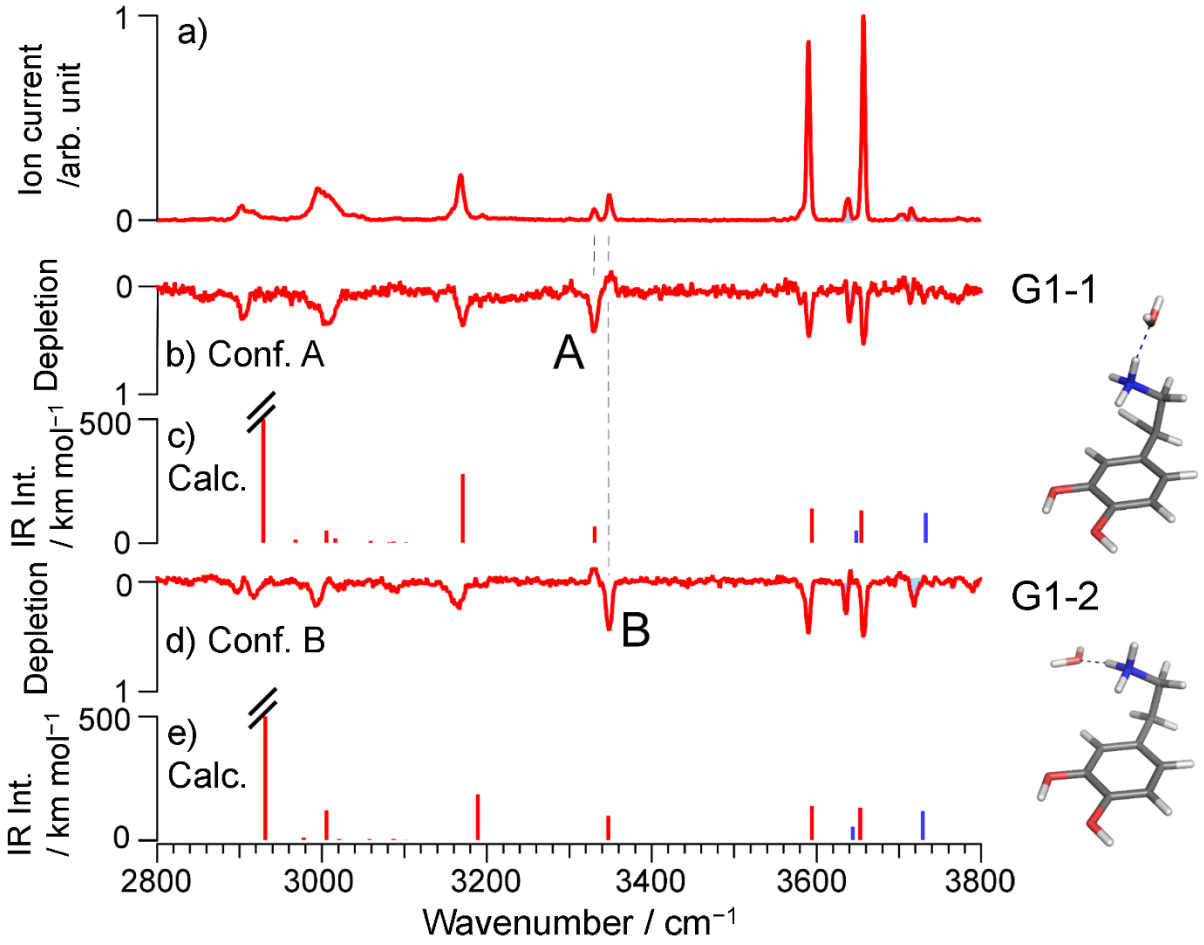

Fig. 4 a) IRPD and IR-IR dip spectra obtained by probing b) the band at 3330 cm^{-1} indicated by letter A and d) the band at 3349 cm^{-1} indicated by letter B of $DAH^+(H_2O)$. Calculated IR spectra for c) G1-1 and e) G1-2 conformations are shown with its molecular structure.

For these two conformers, the water forms a H-bond either on the top or on the side of the protonated ammonium group, leaving some room for a direct interaction of the ammonium with the catechol ring. The predicted IR spectra of the 4 others low energy conformers of $DAH^+(H_2O)$, lying within 2 kJ/mol of G1-1, are reported in Fig S7. For the G1-3 and G2-2 conformers, the water molecule is inserted in between the NH_3^+ and the aromatic ring. Interestingly, those two conformers lack of predicted vibrational transitions around 3180 cm^{-1} in contradiction with the experimental spectra. Besides, the inserted water molecule would certainly prevent fast and efficient excited state proton transfer. Conformers G1-3 and G2-2 are thus excluded from the assignment. The last two conformers G2-1 and G2-3 indeed correspond to the anti conformer (the

$2\pi/3$ rotamer along the C_α-C_β bond) of the G1-1 and G1-2, respectively. The IR frequencies are barely sensitive to the orientation of the alkyl chain above the catechol ring, except the NH stretch pointing towards the catechol around 3160-3190 cm^{-1} (NH_3 sym for G1-1 and G1-2). In the IR-IR dip spectrum reported in Fig. 4d, the unresolved splitting of the experimental transition at 3170 cm^{-1} might be assigned to the coexistence of two rotamers G1-2 and G2-3 which might thus be populated in the cold ion trap.

3.4 IR-IR dip spectra of $DAH^+(H_2O)_2$

The UV spectrum of $DAH^+(H_2O)_2$ is also broad, thus again we will select the conformations which are prone to promote ESPT. Fig. 5a shows the IRPD spectrum of $DAH^+(H_2O)_2$. The vibrational bands are well resolved but the number of bands, particularly around 3350 cm^{-1} suggests the coexistence of at least three conformers. The coexistence of conformers is confirmed by the IR-IR dip spectroscopy. Fig. 5b, 5d and 5f show the IR-IR dip spectra obtained by probing the vibrational bands A, B and C, respectively. These spectra are slightly but clearly different from each other and reproduce all the transitions observed in the IRPD spectrum. Therefore, it can be concluded that $DAH^+(H_2O)_2$ has three different conformers.

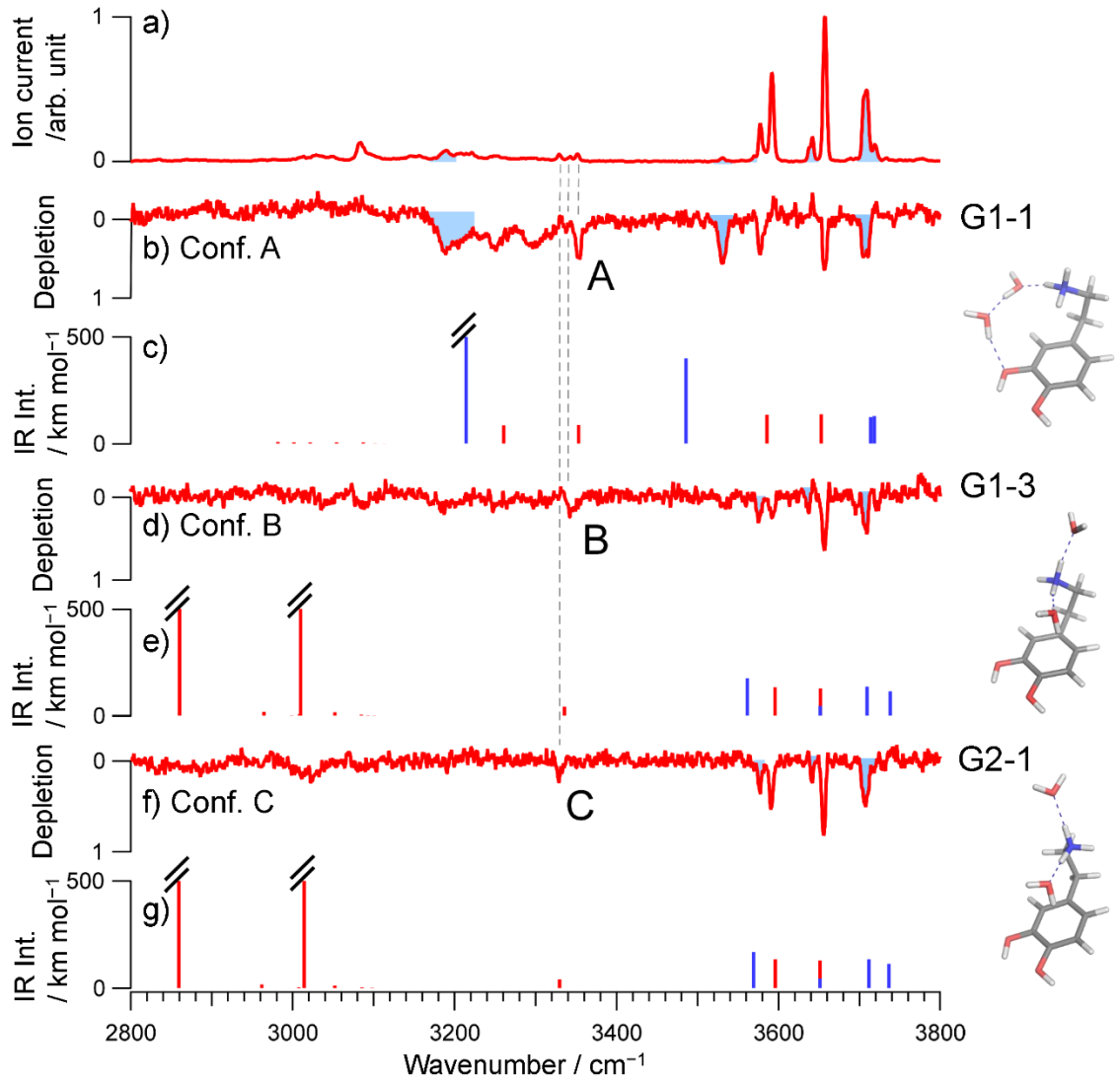

Fig. 5 a) IRPD and IR-IR dip spectra obtained by probing b) the band at 3352 cm^{-1} indicated by letter A, d) the band at 3343 cm^{-1} indicated by letter B and f) the band at 3329 cm^{-1} indicated by letter C of $DAH^+(H_2O)_2$. Calculated IR spectra for c) G1-1, e) G1-3 and g) G2-1 conformations are shown with its molecular structure.

The ten lowest energy conformers of $DAH^+(H_2O)_2$ are reported in Fig. S10 along with their free Gibbs energies at 180 K (Table S3). The predicted spectra of these ten conformers are reported in Fig. S11. The bands originated form water molecules are indicated by blue as they disappear in the IR spectrum of the deuterated complex (Fig. S9). The observed IR spectra of conformers A, B and C are compared to theoretical spectra of G1-1, G1-3 and G2-1 in Fig. 5, respectively. These

theoretical spectra reasonably reproduce the three IR-IR dip spectra. In particular, among the ten lowest energy conformers, only G1-1 has an intense water vibration at 3220 cm^{-1} consistent with broad absorption seen in the experimental spectrum A which disappear in the deuterated complex. It is noteworthy that for conformers G1-2 and G2-2, the three N-H bonds are involved in hydrogen bonding with two water molecules and the catechol ring, respectively. This leads to the lack of free NH stretch around 3325 cm^{-1},[26] in contradiction with the IR-IR dip spectra. So these two conformers can be excluded from the analysis. At the opposite, G1-1, G1-3 and G2-1 have a N–H bond pointing toward a carbon atom of the catechol ring, thus prone to trigger ESPT following the UV excitation.

3.4 Excited state dynamics in $DAH^+(H_2O)_n$

In our recent communication,[11] we reported the fast excited state proton transfer in DAH^+ monomer, which is responsible for the broad feature of the UV spectrum (see Fig. 1). Minimum Energy Path along the N–H^+ stretch bond toward the ring leads to an excited state proton transfer with a low energy barrier of 0.15 eV. We have investigated the ESPT in DAH^+-$(H_2O)_{n=1,3}$ at the SCS-CC2 level by calculating the reaction path connecting the locally excited $^1\pi\pi^*$ state with the proton transferred structures for several conformers of each cluster size.

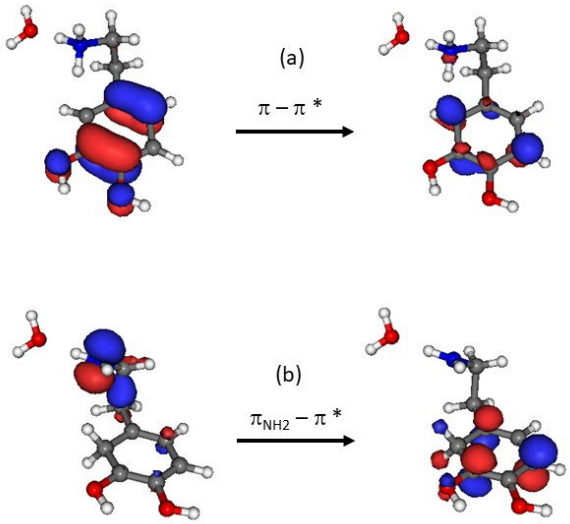

Fig. 6 Molecular orbitals involved in the S_1 state of (a) the locally excited ππ* state and (b) ESPT structure of conformer G1-2 of DAH^+-H_2O complex, which depicts the electronic excitation from

the non-bonding π orbital of the NH_2 group toward the antibonding orbital of the catechol ring.

The exothermic ESPT reaction has already been evaluated in similar systems and ranges from 0.2 eV for protonated Tryptophan[27] to 0.5 eV for protonated Tyrosine and Phenylalanine[6] up to 0.9 eV for protonated adrenaline.[28] In any cases, the HOMO and LUMO molecular orbitals characterizing the ESPT structure are localized on the aromatic ring. However, in the ESPT structure of hydrated dopamine, after geometry optimization, the amino group becomes planar, revealing a change from sp^3 hybridization of the nitrogen atom toward sp^2. It is noteworthy that in the course of the ESPT, the electronic configuration of the first excited state changes from a ππ* transition located on the catechol ring to $\pi_{NH2}\pi_{ring}$* character (see the molecular orbitals plotted in Fig. 6). It should be stressed that the π_{ring}* orbital of the ESPT structure obviously differs from the one of the non-transferred species due to the protonation of the aromatic ring. In the ESPT structure, the highest occupied orbital has the electronic density on the plane of the NH_2 group, which resembles the non-bonding π_{nb} orbital in formamide.[29] As the water cluster size increases, the S_1 state of the ESPT form is further stabilized compared to the locally excited ππ* state from 0.4 eV in the 1-1 complex to 0.7 eV in the 1-3 complex (see Fig. 7). Such a solvation effect has already been observed in formamide,[30] for which the $\pi_{NH2}\pi$* transition undergoes a red shift of up to 1 eV in water as compared with gas phase calculations. The stabilization of the $\pi_{NH2}\pi$* state is induced by the local interaction of the NH_2 with the water molecules, while the locally excited ππ* state of DAH^+-$(H_2O)_n$ is barely affected by solvation because of the lack of direct interaction of the water with the catechol ring. In the hydrated clusters of protonated dopamine, the NH_2 group forms H-bond with at least one water molecule. The alignment of the dipoles of the water and the amide moiety is responsible for the stabilization of the $\pi_{NH2}\pi$* state. For instance, in the G1-2 conformer of $DAH^+(H_2O)$, the vertical excitation energy of the S_1 $\pi_{NH2}\pi$* state is calculated at 1.68 eV while the S_2 ππ* state is located at 2.85 eV, so + 1.15 eV above. Removing the water changes the relative energy of the excited states, the excitation energy of the $\pi_{NH2}\pi$* state increases to 2.15 eV (+ 0.47 eV) while the ππ* excitation energy is only shifted by +0.1 eV.

Solvent not only affects the nature and ordering of excited states, but also the possible deactivation process. The evolution of the excited state energies along the reaction path connecting the locally

excited ππ* state with the $\pi_{NH2}\pi^*$ state of the ESPT form exhibit a low energy barrier of 0.1 eV for all the conformers showing broad UV spectra. However, in the G1-1 conformer of $DAH^+(H_2O)_3$, intramolecular proton transfer from the ammonium to the catechol ring is prevented by the hydration of three water molecules. As reported in ref 11, stretching the N-H^+ bond toward the water inserted in between the ammonium and catechol groups in order to induce a two-step proton transfer exhibits a high barrier which prevents the reaction to take place. Thus, the sharp, well-resolved spectral feature of the conformer A of $DAH^+(H_2O)_3$ is consistent with the assignment of conformer G1-1. In contrast, the proton transfer is highly possible in G1-2, because the NH – ring distance is significantly smaller than that in G1-1 (2.7 Å vs 3.1 Å, respectively). Furthermore, there is no water between NH^+ and the ring in G1-2, thus the proton can access directly the ring. The theoretical calculation also supports ESPT in G1-2. Fig. 7 displays the evolution of the excited state energy along the reaction path connecting the locally excited ππ* to the $\pi_{NH2}\pi^*$ for the G1-2 conformations of DAH^+-H_2O and DAH^+-$(H_2O)_3$. For both cluster sizes, the optimized reaction paths exhibit a low energy barrier height (0.1 eV) that strongly suggests an efficient excited state proton transfer reaction.

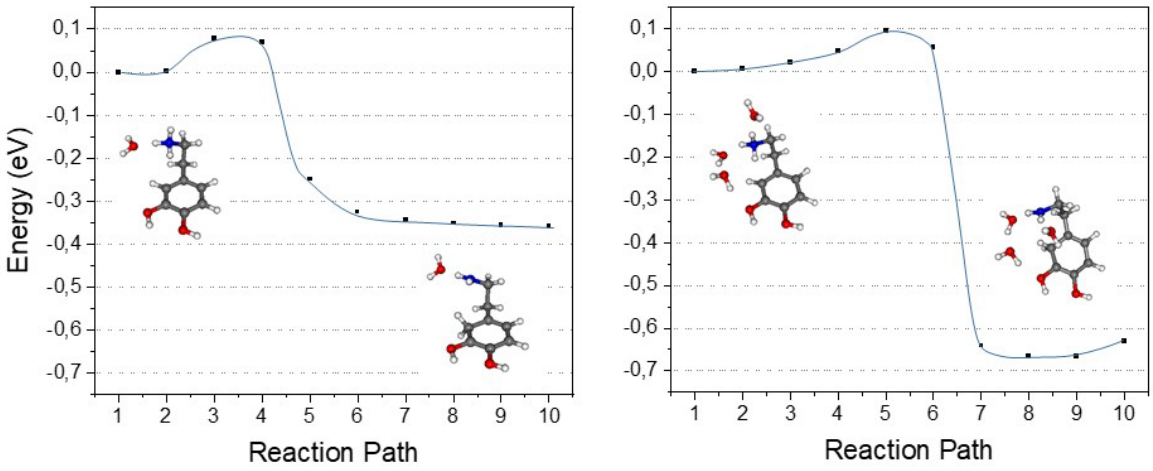

Fig. 7 Optimized reaction paths (SCS-CC2/aug-cc/pVDZ) connecting the locally excited state $^1\pi\pi^*$ with the the $\pi_{NH2}\pi^*$ state for G1-2 $DAH^+(H_2O)$ and $DAH^+(H_2O)_3$. Energy (eV) compared to the adiabatic $^1\pi\pi^*$ excitation transition of each conformer.

Finally, while water evaporation dominates the photodissociation mass spectra for all cluster size, a new fragmentation channel opens for the G1-1 $DAH^+(H_2O)_3$. H-loss channel is detected only

from this conformer since the well-resolved vibronic transitions are recorded while monitoring this channel (Fig. S1). H-loss, a specific UV photofragment following electronic excitation in protonated molecules has already been largely documented.[31] It relies on the electronic coupling between the locally excited ππ* state with a dissociative πσ* state for which the antibonding σ_{NH}* orbital is centered around the ammonium group. In $TrpH^+(H_2O)_n$ clusters, Rizzo and coworkers have shown that in the 1-2 complex, all three of the ammonium NH bonds are involved in H-bonds with two water molecules and the carboxyl group.[32] The transition to the σ* orbital is thus shifted by more than 1 eV. Besides, the water molecules block the ESPT responsible for the broad excitation spectrum of $TrpH^+$ at the band origin.[27] Interestingly, in the G1-1 conformer of $DAH^+(H_2O)_3$, the H-bond network of the water clusters around the dopamine leaves a free NH moiety pointing upward. Vertical excitation energies have been calculated for this conformer. The S_2 πσ* state lies 1.1 eV above the S_1 ππ*. Geometry optimization of the S_2 πσ* state reduces the πσ*/ππ* energy gap down to 50 meV, but its adiabatic energy stays 0.5 eV above the ππ* band origin. In the G1-1 $DAH^+(H_2O)_3$ conformer, stretching the N-H bond not involved in H-bond from the equilibrium geometry (1.04 Å) to 1.1 Å inverses the ππ*/πσ* state ordering, the latter becoming the S_1 state. The reaction path for the H-loss reaction has thus been estimated through minimum energy path (MEP) calculations for fixed N-H bond distance, i. e., for a given N-H distance, all remaining coordinates being optimized in the S_1 state. The adiabatic energies of the S_0, πσ* and ππ* states as a function of the N-H bond distance are reported in Fig. S12. While the ground state and ππ* state energies increase with the N-H bond distance, the energy of the S_1 πσ* state remains relatively stable. At long N-H distance (from 1.6 Å), the πσ* state would cross the ground electronic state, point where the CC2 calculations are stopped due to convergence failure. The lowering of the πσ* state is consistent with the opening of the H-loss channel while the relatively small ππ*/πσ* barrier ensures that a well-resolved vibronic spectrum for the G1-1 conformer. It should however be stressed that the πσ*/S_0 crossing is estimated about 0.5 eV above the adiabatic excitation energy of the ππ*, so we cannot firmly assert that this specific reaction path is responsible for the opening of the H-loss channel in $DAH^+(H_2O)_3$.

4 Conclusions

In conclusion, we have evidenced the drastic hydration effect on the photophysics of DAH^+

embedded in small water clusters. ESPT reaction caused the broadening of the electronic excitation spectra of protonated hydrated dopamine cluster up to 2 water molecules. Solvation induces a drastic modification of the electronic configuration of the ESPT form, which changes from a ππ* transition involving π electrons of the catechol ring to $\pi_{NH2}\pi^*$ transition. In the hydrated clusters, the H-bond formed between the NH_2 group with the water molecules is responsible for the stabilization of the $\pi_{NH2}\pi^*$ state as the cluster size increases, providing a driven force for the ESPT. From three water molecules, the lowest energy conformer exhibits a sharp, well-resolved vibronic spectrum. In this conformer, the three water molecules form with the ammonium group a rigid square structure that prevents the direct interaction of the proton with the catechol ring. In this conformer, ESPT is blocked while the strong H-bond network form by the three water around the ammonium group certainly avoids large geometry change in the excited ππ* state, which leads to a well-resolved vibronic spectrum. Further works are under progress to build a clustering trap in Orsay in order to record pump-probe photodissociation spectroscopy on hydrated dopamine clusters. By this way, we would be able to record the excited state lifetime of hydrated species and then assert whether or not the broadening of the excitation spectra recorded for the small cluster sizes is related to fast deactivation processes as for the bare dopamine or due to vibronic congestion and bad Franck-Condon factors or a combination of both.

Conflicts of interest

There are no conflicts to declare

Supplementary Material

Gibbs free energy of the DAH^+-$(H_2O)_{n=1-3}$ clusters, IR spectra of the deuterated water clusters, structures and predicted IR spectra of the lowest energy conformers of DAH^+-$(H_2O)_{n=1-3}$ clusters.

Acknowledgements

This work was supported in part by KAKENHI (JP19K23624, JP20K20446, JP20H00372, JP21H04674, and JP21K14585), the Core-to-Core program (JPJSCCA20210004) from Japan Society for the Promotion of Science) of JSPS, the World Research Hub Initiatives in Tokyo

Institute of Technology, the Cooperative Research Program of the ‘‘Network Joint Research Center for Materials and Devices’’ from the Ministry of Education, Culture, Sports, Science and Technology (MEXT), Japan, and the RIKEN Pioneering Project, ‘‘Fundamental Principles Underlying the Hierarchy of Matter: a Comprehensive Experimental Study’’. The computations were performed at the Research Center for Computational Science, Okazaki, Japan, the HPC resources from the “Mésocentre” computing center of CentraleSupélec and École Normale Supérieure Paris-Saclay supported by CNRS and Région Île-de-France (http://mesocentre.centralesupelec.fr/) and the HPC resources MAGI from University Paris 13.

Data availability

The data that support the findings of this study are available from the corresponding author upon reasonable request.

References

1. A. L. Sobolewski, W. Domcke, C. Dedonder-Lardeux and C. Jouvet, *Phys. Chem. Chem. Phys.*, 2002, **4**, 1093-1100.
2. S. Ishiuchi, K. Daigoku, M. Saeki, M. Sakai, K. Hashimoto and M. Fujii, *J. Chem. Phys.*, 2002, **117**, 7077-7082.
3. M. N. R. Ashfold, B. Cronin, A. L. Devine, R. N. Dixon and M. G. D. Nix, *Science*, 2006, **312**, 1637-1640.
4. G. A. Pino, A. N. Oldani, E. Marceca, M. Fujii, S. Ishiuchi, M. Miyazaki, M. Broquier, C. Dedonder and C. Jouvet, *J. Chem. Phys.*, 2010, **133**, 124313.
5. C. Jouvet, M. Miyazaki and M. Fujii, *Chem. Sci.*, 2021, **12**, 3836-3856.
6. G. Féraud, M. Broquier, C. Dedonder, C. Jouvet, G. Grégoire and S. Soorkia, *J. Phys. Chem. A*, 2015, **119**, 5914-5924.
7. A. L. Sobolewski and W. Domcke, *J. Phys. Chem. A*, 2007, **111**, 11725-11735.
8. A. Lagutschenkov, J. Langer, G. Berden, J. Oomens and O. Dopfer, *Phys. Chem. Chem. Phys.*, 2011, **13**, 2815-2823.
9. C. Cabezas, I. Peña, J. C. López and J. L. Alonso, *J. Phys. Chem. Lett.*, 2013, **4**, 486-490.
10. Y. T. Chien Ellen, W. Liu, Q. Zhao, V. Katritch, G. Won Han, A. Hanson Michael, L. Shi, H. Newman Amy, A. Javitch Jonathan, V. Cherezov and C. Stevens Raymond, *Science*, 2010, **330**, 1091-1095.
11. K. Hirata, K. Kasai, G. Grégoire, S. Ishiuchi and M. Fujii, *J. Chem. Phys.*, 2021, **155**, 151101.
12. S. Ishiuchi, H. Wako, D. Kato and M. Fujii, *J. Mol. Spectrosc.*, 2017, **332**, 45-51.
13. B. M. Marsh, J. M. Voss and E. Garand, *J. Chem. Phys.*, 2015, **143**, 204201.
14. E. Sato, K. Hirata, J. M. Lisy, S. Ishiuchi and M. Fujii, *J. Phys. Chem. Lett.*, 2021, **12**, 1754-1758.
15. H. Kang, G. Féraud, C. Dedonder-Lardeux and C. Jouvet, *J. Phys. Chem. Lett.*, 2014, **5**, 2760-2764.
16. S. Grimme, C. Bannwarth and P. Shushkov, *J. Chem. Theory Comput.*, 2017, **13**, 1989-2009.
17. P. Pracht, F. Bohle and S. Grimme, *Phys. Chem. Chem. Phys.*, 2020, **22**, 7169-7192.
18. R. Ahlrichs, M. Bär, M. Häser, H. Horn and C. Kölmel, *Chem. Phys. Lett.*, 1989, **162**, 165-169.
19. S. Ishiuchi, Y. Sasaki, J. M. Lisy and M. Fujii, *Phys. Chem. Chem. Phys.*, 2019, **21**, 561-571.
20. T. Negoro, K. Hirata, J. M. Lisy, S. Ishiuchi and M. Fujii, *Phys. Chem. Chem. Phys.*, 2021, **23**,

12045-12050.
21. O. Christiansen, H. Koch and P. Jørgensen, *Chem. Phys. Lett.*, 1995, **243**, 409-418.
22. R. Ahlrichs, *Phys. Chem. Chem. Phys.*, 2004, **6**, 5119-5121.
23. A. Hellweg, S. A. Grün and C. Hättig, *Phys. Chem. Chem. Phys.*, 2008, **10**, 4119-4127.
24. R. A. Kendall, T. H. Dunning and R. J. Harrison, *J. Chem. Phys.*, 1992, **96**, 6796-6806.
25. C. M. Western, *J. Quant. Spectrosc. Radiat. Transf.*, 2017, **186**, 221-242.
26. J. A. Stearns, S. Mercier, C. Seaiby, M. Guidi, O. V. Boyarkin and T. R. Rizzo, *J. Am. Chem. Soc.*, 2007, **129**, 11814-11820.
27. G. Grégoire, C. Jouvet, C. Dedonder and A. L. Sobolewski, *J. Am. Chem. Soc.*, 2007, **129**, 6223-6231.
28. J. Dezalay, M. Broquier, S. Soorkia, K. Hirata, S.-i. Ishiuchi, M. Fujii and G. Grégoire, *Phys. Chem. Chem. Phys.*, 2020, **22**, 11498-11507.
29. N. A. Besley and J. D. Hirst, *J. Phys. Chem. A*, 1998, **102**, 10791-10797.
30. N. A. Besley and J. D. Hirst, *J. Am. Chem. Soc.*, 1999, **121**, 8559-8566.
31. S. Soorkia, C. Jouvet and G. Grégoire, *Chem. Rev.*, 2020, **120**, 3296-3327.
32. S. R. Mercier, O. V. Boyarkin, A. Kamariotis, M. Guglielmi, I. Tavernelli, M. Cascella, U. Rothlisberger and T. R. Rizzo, *J. Am. Chem. Soc.*, 2006, **128**, 16938-16943.